Environmental Sciences Europe

RESEARCH

Open Access

Irrigation expansion has kept pace with the CO_2 fertilization effect on vegetation growth in a typical arid region

Xiaoyao Lu[1,2,3], Lu Zhang[4,5], William J. Davies[6], Minzhong Zou[1,2,3], Jun Niu[1,2,3], Jinliang Chen[1,2,3], Risheng Ding[1,2,3], Sien Li[1,2,3] and Shaozhong Kang[1,2,3*]

Abstract

Dynamics of vegetation in arid areas have drawn worldwide attention. The expansion of irrigated cropland (ICE) in arid regions contributes to increased food security and impacts on the extent and development of regional vegetation. However, the quantitative attribution of vegetation growth variation from ICE and biogeochemical factors (e.g., atmospheric CO_2 concentration, climatic factors) is still lacking. Here, we assessed key drivers of vegetation growth in the inland arid region of Northwest China (IANC) from 1982 to 2018, including ICE, increased nitrogen rates, elevated atmospheric CO_2 concentration (eCO_2) and climate drivers, using normalized difference vegetation index (NDVI) and ecosystem gross primary productivity (GPP) as measures. These variables were quantified through trend decomposition, machine learning algorithms, and a satellite-based model. The results show that vegetation growth was increased in IANC mainly due to eCO_2 and ICE. After 1995, as the regional climatic aridity intensified, the CO_2 fertilization effect on vegetation growth decreased, as the atmospheric CO_2 concentration continued to increase. Meanwhile, irrigated cropland area increased sharply, and ICE-driven GPP variation exceeded that driven by eCO_2 in the whole region, while the ICE-driven NDVI variation exceeded that due to eCO_2 when the ICE reached 6.38%. The ICE effect on regional vegetation growth rather than the CO_2 fertilization effect has mitigated the slowdown of the rate of vegetation growth caused by climate changes. Although the ICE is conducive to food security and continuous greening of arid areas, further reclamation will exacerbate water scarcity. Our results provide research base for identifying the scale of sustainable agricultural development.

Highlights

- Vegetation growth was enhanced in Northwest China mainly due to the CO_2 fertilization effect and irrigation expansion during 1982–2018.
- The effect of irrigation on vegetation growth approached or even outweighed that of elevated atmospheric CO_2 concentration after 1995.
- The effect of irrigation expansion mitigates the slowdown of vegetation growth trend, instead of the CO_2 fertilization effect.

Keywords Irrigated cropland expansion, Arid regions, CO_2 fertilization effect, NDVI, GPP, Climate changes

*Correspondence:
Shaozhong Kang
kangsz@cau.edu.cn
Full list of author information is available at the end of the article

Springer Open

© The Author(s) 2024. **Open Access** This article is licensed under a Creative Commons Attribution 4.0 International License, which permits use, sharing, adaptation, distribution and reproduction in any medium or format, as long as you give appropriate credit to the original author(s) and the source, provide a link to the Creative Commons licence, and indicate if changes were made. The images or other third party material in this article are included in the article's Creative Commons licence, unless indicated otherwise in a credit line to the material. If material is not included in the article's Creative Commons licence and your intended use is not permitted by statutory regulation or exceeds the permitted use, you will need to obtain permission directly from the copyright holder. To view a copy of this licence, visit http://creativecommons.org/licenses/by/4.0/.

Introduction

Satellite observations have shown that since the 1980s, global vegetation has exhibited an overall greening. Despite this, some areas show browning trends [5, 28, 32, 50, 56]. After the mid-1990s, due to the intensification of drought condition, the intensity and extent of vegetation browning expanded, resulting in a stalling or reversal of vegetation greening in different parts of the world [28, 31, 50]. Although the trends of vegetation growth in some regions have declined, there are still regions that continue greening as a result of land-use management. In recent years, to protect and restore degraded forest ecosystems, many countries have implemented a series of forest restoration projects, such as the Three North Shelterbelt Development Program and the Grain to Green Program in China, the New York Forest Declaration and the Bonn Challenge [4, 20, 39, 52]. In addition, expanding the sown area through irrigation and fertilization increases crop yield [25], which not only enhances food security, but also promotes regional greenness. Studies have shown that since 2000, the increase in global vegetation growth is mainly caused by the greening of forests and cropland [4]. Many studies have attached great importance to the impact of afforestation on regional vegetation growth [4, 21, 33, 40]. However, the quantitative effects of expansion of irrigated cropland (ICE) on NDVI and GPP are still uncertain.

Vegetation growth dynamics are influenced by a combination of factors, including biogeochemical factors, as well as land-use-related drivers (e.g., land use changes and agricultural management measures) [32, 56]. Globally, elevated atmospheric CO_2 concentration (eCO_2) is considered to be the most important driver of vegetation greening [56]. In arid regions, climate change has had an important impact on vegetation growth [9, 26, 56]. Recently, as atmospheric CO_2 concentration continues to increase, the warming-induced atmospheric aridity is intensifying, which generates a negative impact on vegetation growth [27, 31, 50]. Studies have shown that the physiological response of plants to eCO_2 can enhance leaf photosynthesis, improve water use efficiency [7], and alleviate some of the impact of atmospheric drought on vegetation growth [2, 48]. However, some studies have reported that enhanced vegetation growth means more water and nutrients consumption, aggravating the water scarcity in arid regions [8, 22], and the CO_2 fertilization effect will decrease due to water and nutrient limitations [17, 38, 42, 44]. These indicate that in drier conditions, the fertilization effect of CO_2 may decrease. A critical gap in our understanding pertains to the synergy and antagonism between different drivers.

The inland arid region of Northwest China (IANC) is located in the hinterland of the Eurasian continent (Additional file 1: Fig. S1a). It is an important strategic place of the ancient and modern 'Silk Road'. It covers an area of 2.115 million km^2, equivalent to about half of the area of the European Union. Four of the eight deserts in China are completely contained in the IANC, and two deserts are adjacent to it. Among them, the Taklimakan Desert is the largest desert in China and the second largest mobile desert in the world. The agriculture in IANC is highly dependent on irrigation, and the oasis agriculture formed at the edge of the desert has become important ecological barrier. Since the mid-1990s, large-scale ICE has taken place to meet the surging food demand, increasing the area of irrigated cropland by about 55% (Additional file 1: Figs. S2b, S3). In addition, over the last few decades IANC has experienced remarkable climatic warming, and the relative humidity decreased significantly after 1990s (Additional file 1: Figs. S2c, S4c), which has had an impact on regional ecological vegetation. It is urgent to clarify the impacts of various factors on regional vegetation growth in such an ecologically fragile environment, and it is necessary to explore the interaction between human activities and 'natural' factors, as well as different 'natural' factors to ensure food security and ecological health in this and other arid regions. In this paper, satellite-based GIMMS3g NDVI and MODIS NDVI data sets were used to show the greening pattern in IANC from 1982 to 2018. We then quantified the effects of biogeochemical factors (including atmospheric CO_2 concentration and climate) and land-use-related drivers (including ICE and change of nitrogen fertilization per unit area) on IANC's NDVI variation in the growing season (from May to October). This was achieved through trend decomposition and three machine learning algorithms. In addition, the cumulative GPP in the growing season was calculated using a revised remote sensing-based light use efficiency (LUE) model, and model experiments were performed to quantify the effects of various factors on ecosystem productivity.

Methods

Data sets

The data used in this paper include satellite remote sensing data, meteorological data, reanalysis data, and statistical yearbook data. The time period, temporal and

spatial resolutions, and sources of the data are shown in Additional file 1: Table S1.

Vegetation greenness

As an indicator of vegetation greenness, the satellite-based NDVI data was used in this study, including the GIMMS3g NDVI and the MOD13A3 NDVI (see details in Additional file 1: Table S1). The multi-year monthly average values of GIMMS3g NDVI in IANC were calculated, and the months with NDVI greater than 0.1 were designated as the growing season (from May to October). The growing season NDVI was integrated by taking the average value from May to October. The GIMMS3g NDVI is represented on a resolution of 0.0833°. The MOD13A3 NDVI was resampled to the same spatial resolution as the GIMMS3g NDVI by the nearest neighbour method, and the variation and magnitude of the GIMMS3g NDVI and the MOD13A3 NDVI were almost the same in the study area (Additional file 1: Fig. S5). Therefore, the MOD13A3 NDVI was used to supplement the GIMMS3g NDVI to obtain vegetation greenness information for a longer time period (1982–2018).

Human activities

Two land use data sets (see Additional file 1: Table S1 for details) were collected as indicators of spatial change in regional irrigated cropland area from 1982 to 2018, and the irrigated cropland area and its changes displayed in these two sets of data are highly consistent (Additional file 1: Fig. S3). By summing the cropland area of all 0.00833° pixels in each 0.0833° pixel, the data were aggregated to the same spatial resolution as the NDVI data.

We used data on nitrogen application per unit area in Xinjiang and the Hexi Corridor from the Xinjiang Statistical Yearbook and the Gansu Development Yearbook. In addition, spatial nitrogen application data were obtained from a global data set [23]. There was a significant linear correlation between the nitrogen fertilization data in the statistical yearbook and the global data set (Additional file 1: Fig. S6a), so the statistical yearbook data were used to correct and extend the data in the global data set.

Meteorological data and atmospheric CO_2 concentration data

Meteorological data mainly came from the China National Meteorological Center. The data collected at 110 meteorological stations were interpolated to 0.0833° spatial grid data using the nearest neighbor method. The cumulative solar radiation for the growing season was calculated from the solar radiation data in the re-analyzed data set and the record of sunshine hours from the meteorological stations.

Atmospheric CO_2 concentration data observed at the Global Atmospheric Background Station at Waliguan was obtained from the National Cryosphere Desert Data Center. Waliguan Station is the only atmospheric background observation station in the inland region of the Northern Hemisphere, and its observations reflect the atmospheric greenhouse gas concentrations and their changes in the mid-latitude inland regions of the Northern Hemisphere. In addition, longer observation from the Mauna Loa Observatory was obtained from the Global Monitoring Laboratory. The interannual variations in CO_2 data from the two stations were highly consistent (Additional file 1: Fig. S6b), so the observations from Mauna Loa Observatory were used in calculations.

Trend change point detection

The Akaike Information Criterion (AIC) and segmented regression [1] (a linear regression that modifies its slope at a certain value of the predictor, or threshold) were used to determine the trend change points of interannual variations of observation elements. We used AIC to choose the model that best-fitted the data. When nonlinear regression (e.g., quadratic function) was a better fit to the data, trend change point may be present, and in these cases, the trend change point is defined by segmented regression. The segmented regressions were achieved through the 'SiZer' package in R, and the bootstrap sampling on each database was set 1000 times, with a confidence interval of 95%.

After AIC judgement, we found that there were trend change points in the trends of 'growing season' mean GIMMS3g NDVI in the natural vegetation zone, the irrigated cropland area, and the relative humidity. The trend change points of the above three elements are 1990, 1995 and 1992 respectively (Additional file 1: Fig. S2). We selected 1995 as the dividing point between the early and later periods, because 1995 is not only the change point for the trend in irrigated cropland area, but also falls within the 95% confidence interval of the trend change points for natural vegetation NDVI and relative humidity (Additional file 1: Fig. S2).

Effect of ICE on NDVI calculated by trend decomposition

We used the trend decomposition method to quantify the effect of ICE on NDVI. We use a linear trend to represent the change in NDVI over a period of time. First, we calculated the growing season NDVI trend of each 0.0833° pixel ($pel_{0.0833}$) from1982 to 2018. Secondly, the $pels_{0.0833}$ with the proportion of cropland greater than 10% were identified as cropland pixels in 1982 and 2018, and then

the cropland change pixels between 1982 and 2018 (hereinafter referred to as ICE pixels) were identified (Additional file 1: Fig. S7a). The $pels_{0.0833}$ with the proportion of natural vegetation (uncultivated vegetation) greater than 60% coverage, both in 1982 and 2018, were defined as natural vegetation pixels. The proportions of cropland and natural vegetation were derived from the land use data products. We then decomposed the NDVI trends of ICE pixels by considering two cases:

a) If there was natural vegetation in the ICE pixel before 1982, it was considered that the NDVI variation trend caused by ICE was the actual NDVI trend minus the reference trend value [Eq. (1)].
b) If there was no natural vegetation in the ICE pixel before 1982, it was considered that the variation of NDVI was caused by ICE [Eq. (2)]:

$$Trend'_{ICE} = Trend_{actrual} - Trend_{ref} \quad (1)$$

$$Trend'_{ICE} = Trend_{actrual} \quad (2)$$

Where $Trend'_{ICE}$ represents the NDVI trend caused by ICE in the ICE pixel, $Trend_{actrual}$ represents the actual NDVI trend in the corresponding $pel_{0.0833}$, and $Trend_{ref}$ represents the reference trend value which is calculated at the grid with spatial resolution of 0.75° ($grid_{0.75}$) (Additional file 1: Fig. S7c). Each $grid_{0.75}$ contains 81 $pels_{0.0833}$. The $Trend_{ref}$ is calculated by averaging the NDVI trends of all natural vegetation pixels in the $grid_{0.75}$. It should be noted that we assume that at each $grid_{0.75}$, all $pels_{0.0833}$ have the same climate background and are taken to have experienced the same agricultural management measures. Through the above operation, we calculated the effects of ICE on NDVI in ICE pixels. However, the $pels_{0.0833}$ that had cropland before 1982 and the $pels_{0.0833}$ with small change in the irrigated cropland area were ignored. Where there was a significant linear correlation between cropland area change and NDVI variation (Additional file 1: Fig. S7b), the NDVI variation caused by ICE was spatially extrapolated through the actual irrigated cropland proportion of change of the $pel_{0.0833}$ and the $\overline{Trend}^0_{ICE}$ of the $grid_{0.75}$ where the $pel_{0.0833}$ is located [Eqs. (3), (4)]:

$$Trend^0_{ICE} = Trend'_{ICE} / ICE'_{actual} \quad (3)$$

$$Trend_{ICE} = \overline{Trend}^0_{ICE} \times ICE_{actual} \quad (4)$$

where ICE'_{actual} is actual cropland proportion changes of the ICE pixels; $Trend^0_{ICE}$ is the NDVI trend caused by the change of unit cropland proportion in the ICE pixels, and the $\overline{Trend}^0_{ICE}$ is the average value of $Trend^0_{ICE}$ in a $grid_{0.75}$; $Trend_{ICE}$ is the NDVI trend caused by the ICE (Additional file 1: Fig. S7d), and ICE_{actual} is the actual irrigated cropland proportion changes in the $pels_{0.0833}$.

Machine learning algorithms for estimating the effects of various factors on NDVI

Three machine learning algorithms (Additional file 1: Table S2) were used to model and estimate NDVI with variation in different biogeochemical factors (atmospheric CO_2 concentration, photosynthetically active radiation, relative humidity and air temperature) and human activities (irrigated cropland area, nitrogen fertilization). Satellite-derived growing season mean NDVI data were used for model training and verification. If the numbers of target data are small, the machine learning algorithm may 'over fit'. Therefore, we used $grid_{0.75}$ as the calculation unit to expand the sample size. We had 81 $pels_{0.0833}$ in each $grid_{0.75}$, and each $pel_{0.0833}$ contained 35 years of data, that is, there were 2835 samples at each $grid_{0.75}$ for model construction. 70% of the samples were randomly selected for model training and the remaining 30% for testing. Through the random search and the cross validation, the optimal parameters were selected for each grid. We use the coefficient of determination (R^2) between the simulated values and observed values in the test set as the evaluation metric for the model, and our results suggest that machine learning algorithms can effectively estimate NDVI (Additional file 1: Fig. S8). Among them, the simulation efficiency of the Random Forest and MLP Neural Network is superior to that of the Support Vector Machine. We synthesized the results of the three models by calculating their average.

We calculated the effects of various drivers on variation of NDVI through model experiments. Firstly, we made all factors change over time to calculate $NDVI_{ALL}$ (a normal model run). Next, we kept the variable x constant (e.g., ICE, eCO_2) to calculate $NDVI_x$ with other factors changing over time. The difference between $NDVI_{ALL}$ and $NDVI_x$ is the NDVI variation driven by variable x:

$$\Delta NDVI_{xi} = NDVI_{ALLi} - NDVI_{xi} \quad (5)$$

where $\Delta NDVI_{xi}$ is the NDVI variation driven by variable x in the ith year. The trend of NDVI driven by x was calculated by the least square method. The sensitivity of NDVI to the ICE was analyzed through linear regression. The calculation equation is as follows:

$$\Delta NDVI_{ICEk} = \gamma_{ICE} \times \Delta ICE_k + \varepsilon \quad (6)$$

where $\Delta NDVI_{ICEk}$ is the NDVI variation driven by ICE between 1982 and 2018 in the kth $grid_{0.75}$, and ΔICE_k is ICE proportion (i.e., the proportion of irrigated cropland area to total vegetation area between 1982 and 2018) in the kth $grid_{0.75}$; γ_{ICE} is the sensitivity of NDVI to ICE; ε is the residual term.

Regional productivity estimation and attribution

A revised light use efficiency (LUE) model was used to estimate regional productivity of vegetation (GPP), and the calculation equation is as follows [10, 50]:

$$GPP = PAR \times FPAR \times \varepsilon_{max} \times C_s \times T_s \times W_s \quad (7)$$

where PAR is photosynthetically active radiation, calculated as 1/2 of the solar radiation (unit: MJ/m^2/month); FPAR is the fraction of PAR absorbed by the vegetation canopy, which can be calculated by NDVI [Eq. (8)] [3]; ε_{max} is the maximum LUE, and we take the fixed empirical value of 2.76 g C/MJ [12, 37, 50] to prevent the effects of some factors from being repeatedly considered; C_s, T_s and W_s represent the downward-regulation scalars for the respective effects of eCO_2, air temperature and moisture conditions on the LUE [3, 10, 29, 50, 53]. The effect of atmospheric CO_2 concentration on LUE (C_s) was obtained from the work of Yuan et al. [50], and see details in the supplementary information. T_s was calculated by mean air temperature (T_a, unit: °C) and the optimal air temperature which is the average temperature of the month with the largest NDVI in a year [10] (see details in the supplementary information). W_s was calculated using regional evapotranspiration (ET) and potential evapotranspiration [PET, Eq. (9)]. The regional ET was obtained through the GLASS ET product [49] and PET was calculated using the Hargreaves equation [Eq. (10)]:

$$FPAR = 1.24 \times NDVI + 0.618 \quad (8)$$

$$W_s = 0.5 + 0.5ET/PET \quad (9)$$

$$PET = C_o R_a (T_a + 17.8)(T_{max} - T_{min})^{0.5} \quad (10)$$

where T_{max} and T_{min} represent the maximum and minimum air temperature in the calculation period, respectively (unit: °C). R_a is the theoretical solar radiation at the top of the atmosphere (unit: MJ/m^2/month); the C_0 is the conversion coefficient with a value of 9.39×10^{-4}.

In the cropland zone, we made some adjustments to the above LUE model. In addition to natural factors, we also considered the effects of ICE and nitrogen fertilization on GPP. The calculation is as follows:

$$GPP = PAR \times FPAR \times \varepsilon_{max} \times C_s \times T_s \times W_{sICE} \times N_s \quad (11)$$

We found that there was a significant linear correlation between the ICE and regional ET, so we substituted this relationship into Eq. (9) to obtain W_{sICE}:

$$ET = aICE + b \quad (12)$$

$$W_{sICE} = 0.5 + 0.5(aICE + b)/PET \quad (13)$$

here, a and b are the coefficients in the regression equation between ET and ICE, which were quantified by the ET of GLASS products and irrigated cropland area in the land use data set, and each $pel_{0.0833}$ has specific values of a and b. Within a certain range, there is a stable proportional relationship between biomass and GPP [16, 24], so we collected nitrogen fertilization and biomass data for three main crops (corn, wheat and cotton) in IANC to quantify N_s. Wheat, corn, and cotton occupy 22.4%, 15.4%, and 31.8% of the planting area, respectively. Over the years, these three crops together have consistently comprised around 70% of the total cultivated area. The regression relationship between nitrogen fertilization and relative biomass (biomass after nitrogen application divided by biomass without nitrogen application) was established, and the AIC was used for judgment. The results showed that there was a significant quadratic function relationship between nitrogen fertilization and relative biomass (Additional file 1: Fig. S9a). We integrated data of different crops to establish a unified relationship (Additional file 1: Fig. S9b).

The revised LUE model was verified by the GPP observation data for the experimental sites, and the simulated results matched well with the observed values (Additional file 1: Fig. S10). GPP was then calculated by weighted averaging based on the proportions of cropland and natural vegetation in each of the $pels_{0.0833}$:

$$GPP_j = GPP_c \times \rho_c + GPP_{nv} \times \rho_{nv} \quad (14)$$

where GPP_j represents the GPP in the jth $pel_{0.0833}$; GPP_c and GPP_{nv} represent the GPP of cropland and natural vegetation, respectively in the jth $pel_{0.0833}$; ρ_c and ρ_{nv} represent the proportions of cropland and natural vegetation area in the jth $pel_{0.0833}$.

We performed numerical simulations to evaluate the effects of various factors on GPP with the revised LUE model. In the LUE model, various factors affect GPP through two aspects: on one hand, drivers regulate GPP by affecting the FPAR which is calculated directly through NDVI, so we call this path the FPAR variable [Eq. (8)]; on the other hand, GPP is affected by various factors through controlling the downward-regulation scalars (e.g., C_s, T_s) of the LUE, and we call this path LUE variable [Eq. (16)]:

$$GPP = PAR \times FPAR \times LUE \quad (15)$$

$$LUE = f(ICE, eCO2, NFER, RH, T_a) \quad (16)$$

where NFER is the nitrogen fertilization and RH is the relative humidity. In the normal model run, all variables changed with time both in the FPAR path and LUE path, which we called GPP_{ALL}. Next, we calculated GPP_x by allowing other factors to change over time while holding the variable x constant at its initial baseline level in the LUE path and substituting NDVI with the $NDVI_x$ in the FPAR path. $NDVI_x$ was calculated by keeping the variable x to maintain the initial value and other factors to change over time in the machine learning algorithm models mentioned above. The difference between GPP_{ALL} and GPP_x is the GPP variation driven by variable x [Eq. (17)]. In addition, we conducted another set of simulation experiments by substituting NDVI with the $NDVI_x$ in the FPAR path and making all variables change with time in the LUE path, which was named GPP'_x. The difference between GPP'_x and GPP_x is the GPP variation driven by variable x through the LUE path [Eq. (18)]:

$$\Delta GPP_{xi} = GPP_{ALLi} - GPP_{xi} \quad (17)$$

$$\Delta GPP'_{xi} = GPP'_{xi} - GPP_{xi} \quad (18)$$

where ΔGPP_{xi} is the GPP variation driven by variable x in the ith year, and $\Delta GPP'_{xi}$ is the GPP variation driven by variable x through the LUE path. The trend of GPP driven by x was calculated by the least square method. In the same way, the sensitivity of GPP to the change of ICE was analyzed through linear regression:

$$\Delta GPP_{ICEk} = \beta_{ICE} \times \Delta \mathrm{ICE}_k + \varepsilon \quad (19)$$

where ΔGPP_{ICEk} is the GPP variation driven by ICE between 1982 and 2018 in the kth $\mathrm{grid}_{0.75}$, and $\Delta \mathrm{ICE}_k$ is the ICE proportion (i.e., the proportion of the total vegetation area which is irrigated cropland area), a value which changes between 1982 and 2018 in the kth $\mathrm{grid}_{0.75}$; β_{ICE} is the sensitivity of GPP to ICE; ε is the residual term.

Results

Vegetation growth changes in IANC

The GIMMS3g NDVI data showed the interannual variation of the average NDVI during the growing season in IANC, with the trends of NDVI calculated by the least square method, as shown in Fig. 1a, b, c. The trends were tested and the trend change points were determined by the AIC and segmented regressions. From 1982 to 2015, the NDVI increased significantly, especially in the cropland zone (Fig. 1a, b). The NDVI trends are 0.000572 yr^{-1} (p = 3.77e-8) and 0.00154 yr^{-1} (p = 1.5e-11) for the whole area and the cropland zone, respectively. The trend change point was found in the NDVI variation in the natural vegetation zone (mainly woodland and grassland) (Additional file 1: Fig. S2a). Since the 1990s, the growth rate of natural vegetation NDVI has slowed down. The study period was divided into two periods, before and after 1995. The NDVI in the natural vegetation zone increased significantly over the early period (from 1982 to 1995), but the growth trend in the later period (from 1995 to 2018) decreased by 84.4% compared with the early period, and the slope became statistically insignificant (Fig. 1c). Figure 2a, c, d shows the spatial distributions of GIMMS3g NDVI trends. After 1995, the intensity and extent of vegetation browning increased significantly, but the cropland zones in the central part of Northern Xinjiang, the Tarim River Basin, and the central and western Hexi Corridor continued greening (Fig. 2a, c, d, Additional file 1: Fig. S1). In addition, the MOD13A3 NDVI data also shows that from 2001 to 2018, the vegetation greenness in the cropland zone increased significantly during the growing season, and the zones with vegetation browning were mainly concentrated in the mid-range of the Tianshan Mountains and the northern mountainous area of Northern Xinjiang (Fig. 2b, Additional file 1: Fig. S1), which was consistent with the GIMMS3g NDVI result.

We used the revised LUE model to estimate regional GPP [10, 50]. The results of the revised LUE model matched well with the measured GPP at the ground experimental sites, especially in the cropland zone (Additional file 1: Fig. S10). We also verified the result of revised LUE model by comparing it with other GPP products. The cumulative GPP in the growing season estimated by the revised LUE model is close to the GLASS GPP product, and is consistent with the variation of MODIS GPP, but the value is greater than that of MODIS GPP (Additional file 1: Fig. S11).

From 1982 to 2018, the cumulative GPP in the growing season in IANC increased significantly. The GPP trends are 2.77 $g\ \mathrm{C}\ \mathrm{m}^{-2}\ \mathrm{yr}^{-1}$ (p = 9.46e-13) and 9.29 $g\ \mathrm{C}\ \mathrm{m}^{-2}\ \mathrm{yr}^{-1}$ (p = 2.08e-16) for the whole area and the cropland zone, respectively (Fig. 1d, e). After 1995, the growth of GPP in the natural vegetation zone stalled. The increasing rate of GPP at the late period of the natural vegetation zone decreased by 79.1% compared with the early period (Fig. 1f).

Attribution of vegetation growth trend

The relative importance of various factors in the attribution calculated by the three machine learning algorithms are basically consistent (Additional file 1: Fig. S12a), and we integrated the results of the three models by averaging. The machine learning algorithms and trend decomposition method showed similar effects of ICE on NDVI

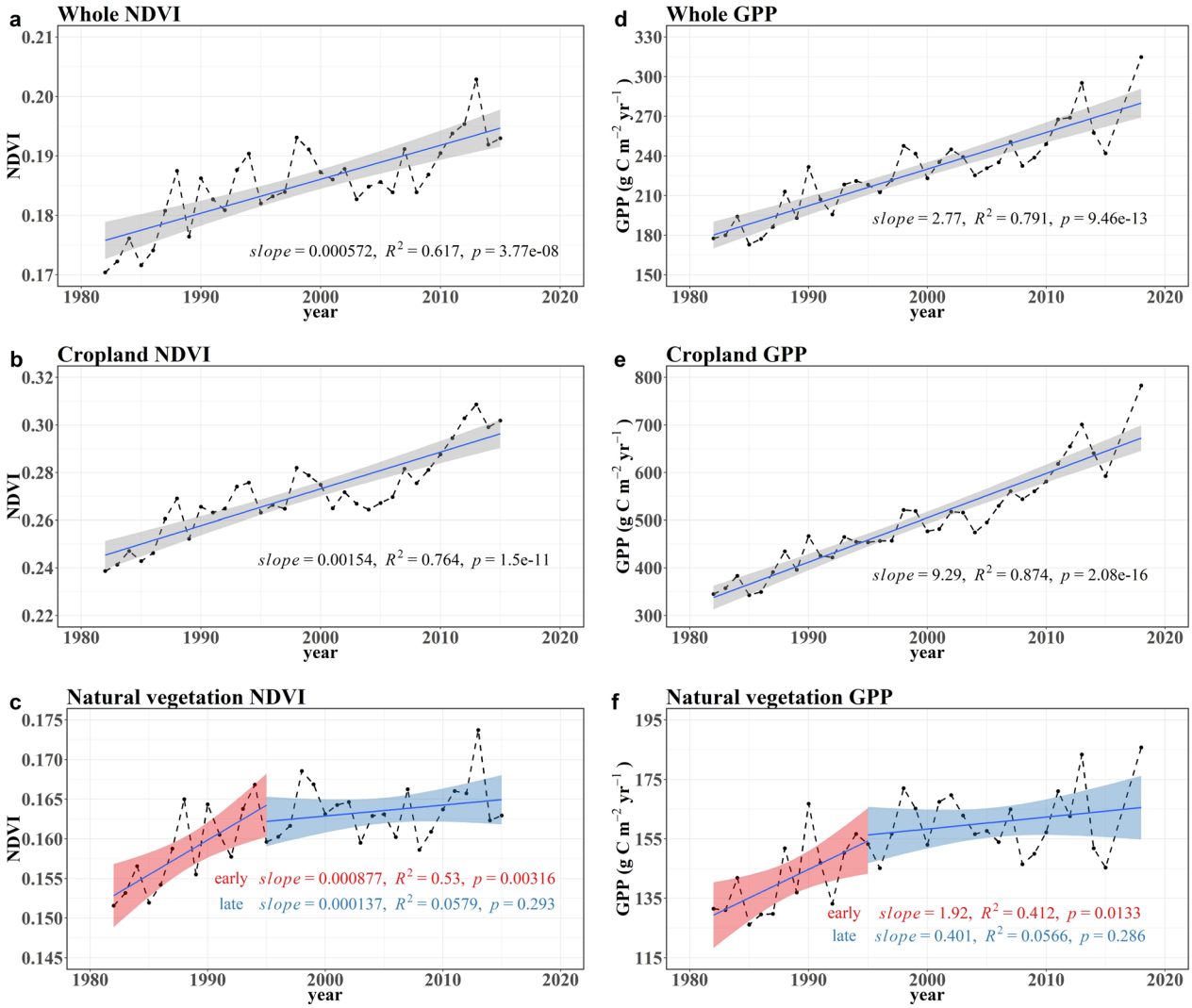

Fig. 1 Variations of vegetation growth in IANC. Interannual variations of growing season (from May to October) mean GIMMS3g NDVI in **a** the whole region, **b** the cropland zone, and **c** the natural vegetation zone. Interannual variations of growing season accumulative GPP calculated by revised LUE model in **d** the whole region, **e** the cropland zone, and **f** the natural vegetation zone. The shaded areas in the figure represent the 95% confidence intervals of the fitted curves. In panels (**c**, **f**), we divided two periods, before and after 1995

(Additional file 1: Fig. S12b). Figure 3 shows the attribution of NDVI trend obtained from the model experiments using the machine learning algorithms. ICE was the dominant factor in NDVI variation in the cropland zone, explaining 61% (61.12 ± 9.78%) of NDVI variation (Fig. 3a). In the natural vegetation zone, NDVI variation was mainly due to eCO_2 (Fig. 3b). Over the whole region, the effect of eCO_2 also dominated, explaining 70% (70.25 ± 7.72%) of the NDVI variation (Fig. 3c). Among the climatic factors, change in relative humidity had the greatest effect on NDVI, and the relative humidity-driven NDVI trend is significantly negative in both cropland zone and natural vegetation zone (Fig. 3a, b). From 1982 to 1995, the regional relative humidity increased, and the NDVI trend driven by relative humidity was positive as well. In the late period (1995–2018), due to the significant decline of regional relative humidity, the NDVI trend driven by relative humidity also became negative (Additional files 1: Figs. S4c and Fig. 3d, e, f). After 1995, the effect of ICE on NDVI trend increased substantially, while the effect of eCO_2 decreased (Fig. 3d, e, f). ICE showed an equally significant effect on NDVI variation as did eCO_2 during the latter part of the study period (ICE: 0.356 ± 0.502, eCO_2: 0.408 ± 0.992, unit: 10^{-3} yr^{-1}) in the whole region (Fig. 3f).

Model experiments were conducted through the revised LUE model to quantify the effects of various

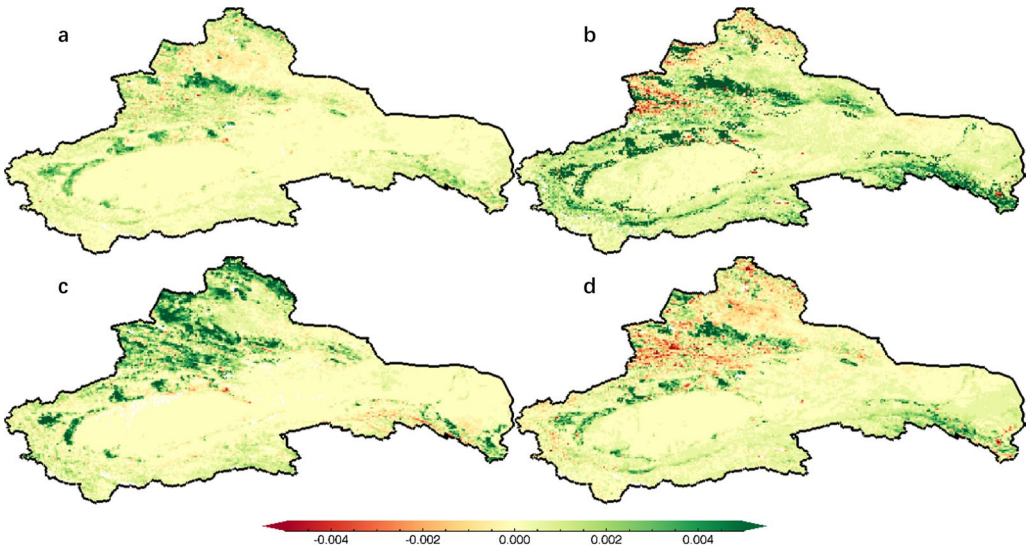

Fig. 2 Spatial patterns of trends in GIMMS3g NDVI in inland arid region of Northwest China (IANC) (unit: $yr.^{-1}$). Growing season mean GIMMS3g NDVI trends during **a** 1982–2015, **c** 1982–1995, and **d** 1995–2015. **b** Spatial patterns of trends in growing season mean MOD13A3 NDVI during 2001–2018

factors on GPP variation. In the cropland zone, ICE is the dominant factor in GPP variation, explaining 58% (57.93 ± 11.66%) of the GPP trend (Fig. 4a). In the natural vegetation zone, as well as the whole region, the eCO_2 had the greatest influence on GPP variation (Fig. 4b, c), which is consistent with the attribution of NDVI trend. However, over the whole region, the contribution of ICE to GPP trend reached 42% (41.99 ± 8.45%), which was close to that of eCO_2 (49.79 ± 12.43%) (Fig. 4c). The effects of various factors on GPP trend were also analyzed in two periods (Fig. 4d, e, f), and the GPP trend driven by relative humidity change was positive at the early period and negative at the late period. The effect of eCO_2 decreased during the late period, while the effect of ICE increased significantly, and the ICE-driven GPP trend over the whole zone exceeded that of eCO_2 at the late period (ICE: 1.30 ± 0.229, eCO_2: 0.800 ± 0.265, unit: g C m^{-2} yr^{-1}) (Fig. 4f).

ICE threshold

The percentage of the change of irrigated cropland area as a function of total vegetation area (ICE proportion) reached 5.25% by 2018. As the ICE proportion grows, the ICE-driven NDVI (or GPP) variation becomes greater, and eventually exceeds the effect of eCO_2. The relationships of the ICE-driven NDVI and GPP variations against ICE proportion between 1982 and 2018 were calculated spatially [Eq. (6), (19)], and showed significant linear correlations (Fig. 5). This means that the sensitivities of NDVI and GPP variations to ICE are consistent in the spatial $grids_{0.75}$, with values of 0.0022 for NDVI and 12.9 for GPP. During the whole period, only if the ICE proportion reaches 10.4%, ICE-driven NDVI variation can exceed the eCO_2 effect in the whole region (Fig. 5a), while the threshold for ICE-driven GPP variation exceeded eCO_2-driven GPP variation is 6.55% (Fig. 5b). Since regional irrigated cropland began to expand after 1995, the ICE-driven vegetation growth variation in the late period was close to that recorded during the entire period. The GPP variation driven by ICE outstripped that by eCO_2 when the ICE proportion exceeded 4.37% in the late period. The ICE-driven NDVI variation reached a level equivalent to the eCO_2 effect in the late period, when the ICE proportion increases to 6.38% (Fig. 5).

Discussion

Effects of ICE on NDVI and GPP

The term 'Vegetation growth dynamics' is often used with reference to changes in vegetation structures and functions, which are affected both by natural drivers and by human activities. As such, such growth dynamics can play a critical role in the material and energy flows of ecosystems [11, 32]. The growth dynamics of vegetation can be quantified by various indicators, such as vegetation greenness, vegetation cover, and ecosystem productivity [13, 21, 45]. Satellite-based NDVI represents vegetation greenness, which can reflect the capacity of vegetation to absorb PAR, as well as the extent of vegetation coverage. The ecosystem productivity quantified by GPP represents the carbon sequestration capacity of vegetation and is an important indicator of the amount of carbon cycling between ecosystems and the atmosphere

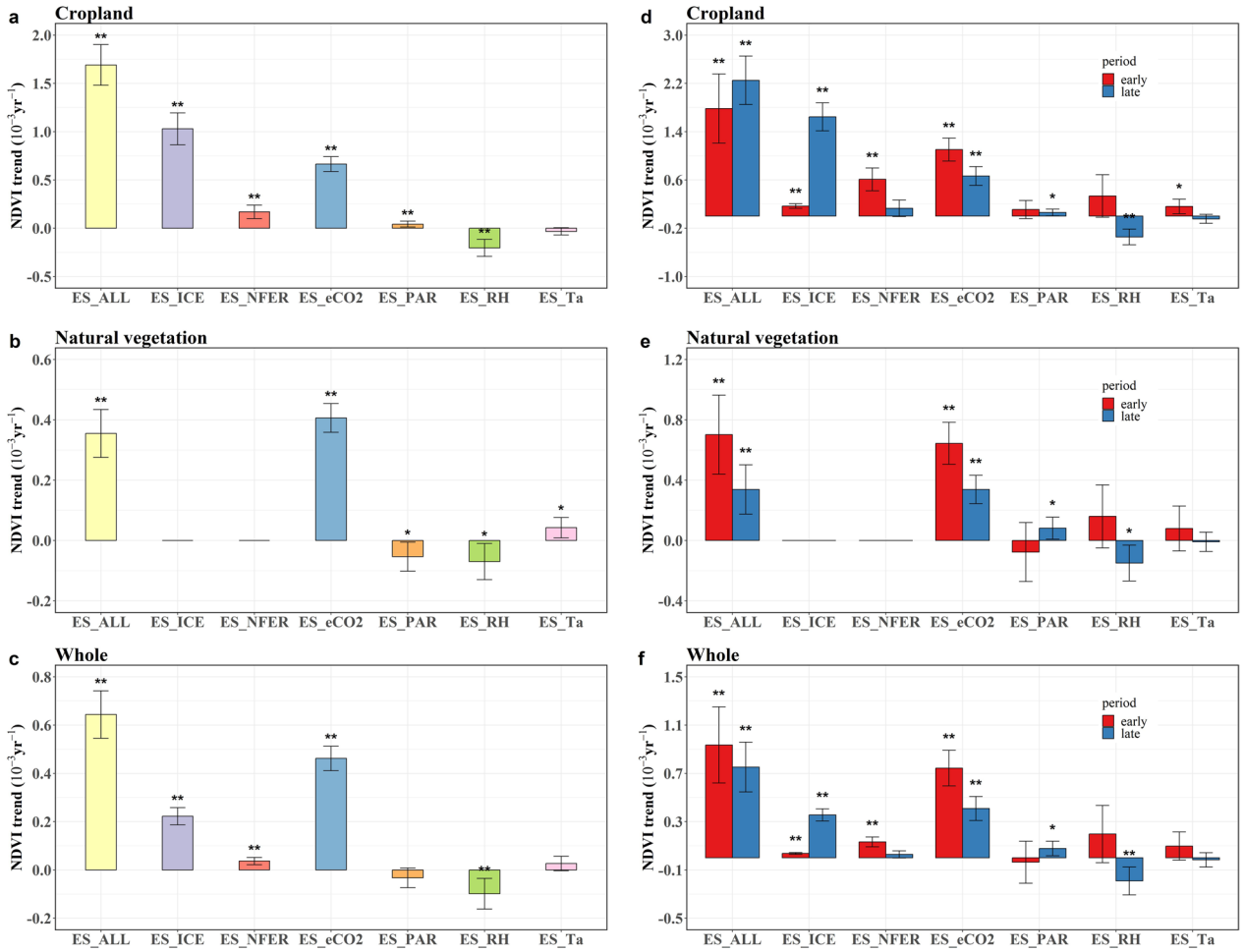

Fig. 3 Attribution of variation in NDVI calculated from model experiments with three machine learning algorithms. In panel (**a**), (**b**), (**c**), the effects of various factors on NDVI in the cropland zone, the natural vegetation zone and the whole region are shown respectively from 1982 to 2018, while panel (**d**), (**e**), (**f**) represent the attribution of NDVI variation in the two periods. The "early" notation indicates the period of 1982–1995, and "late" indicates 1995–2018. The drivers include irrigated cropland expansion (ES_ICE), nitrogen fertilization change (ES_NFER), elevated atmospheric CO_2 concentration (ES_eCO2), photosynthetically active radiation change (ES_PAR), relative humidity change (ES_RH) and air temperature change (ES_Ta). ES_ALL notation indicates the result of model simulation with all factors changing over time. Error bars show the 95% confidence intervals of the trends. Two asterisks indicate that the trend is extremely significant ($P < 0.01$), and one asterisk indicates that the trend is significant ($P < 0.05$)

[6, 36]. The annual precipitation in the desert oasis area in northwest China is less than 200 mm, and the natural vegetation cover is mainly desert steppe and low shrubs [47]. Since the mid-1990s, substantial areas of cropland have been developed and improved in the region through diverting water for irrigation to previously uncultivated areas and to grassy areas in IANC. This has resulted in enhanced vegetation growth regionally. The ICE in IANC supplements the water and nutrient conditions required for vegetation growth through irrigation and fertilization, which promotes regional vegetation greening, increases fixation of CO_2 by plants and further increases ecosystem productivity [43, 51, 55].

After 1995, ICE in IANC had a significant positive effect on regional vegetation growth, and had a greater effect than NDVI on GPP (Figs. 3c, f and 4c, f). In the LUE model, GPP is calculated by multiplying the PAR, FPAR, and LUE [Eq. (15)], where FPAR is related to vegetation greenness and can be estimated by NDVI. The environmental factors that affect FPAR also affect the LUE. Figure S13 shows the GPP trends for the whole region from 1982 to 2018 driven by environmental

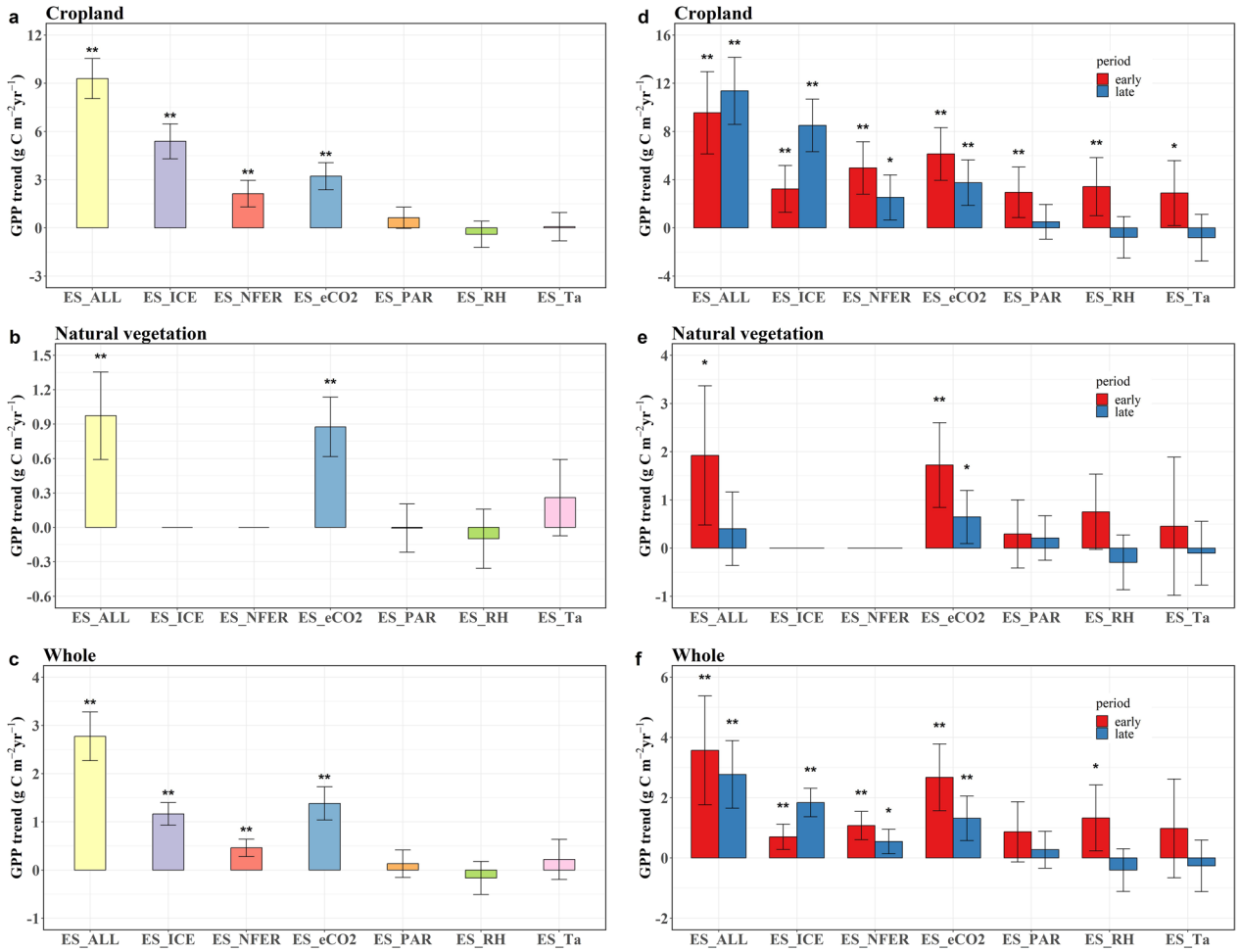

Fig. 4 Attribution of trend in GPP calculated by model experiments of revised LUE model. In panel (**a**), (**b**), (**c**), the effects of various factors on GPP in the cropland zone, the natural vegetation zone and the whole region are shown respectively from 1982 to 2018, while panel (**d**), (**e**), (**f**) represent the attribution of GPP trend in the two periods. The "early" notation indicates the period of 1982–1995, and "late" notation indicates 1995–2018. The drivers include irrigated cropland expansion (ES_ICE), nitrogen fertilization change (ES_NFER), elevated atmospheric CO_2 concentration (ES_eCO2), photosynthetically active radiation change (ES_PAR), relative humidity change (ES_RH) and temperature change (ES_Ta). ES_ALL notation indicates the result of model simulation with all factors changing over time. Error bars show the 95% confidence intervals of the trends. Two asterisks indicate that the trend is extremely significant ($P < 0.01$), and one asterisk indicates that the trend is significant ($P < 0.05$)

variables through effects on LUE. During this period, the ICE contribution was the most significant of that of all driving variables (Additional file 1: Fig. S13c). As a result, ICE not only increases NDVI, which improves the ability of the vegetation canopy to absorb PAR, but more importantly, increases LUE, and further improves regional carbon sequestration.

ICE has slowed the decline of vegetation growth in the region

Plant photosynthesis is enhanced as by the climate change-driven enhancement of atmospheric CO_2 concentration and this can significantly promote vegetation growth. In addition, the physiological response of plant leaves to eCO_2 can improve water use efficiency [7]. Globally, eCO_2 is considered the most important factor in vegetation greening [32, 56]. However, climate change is also increasing air temperatures, crop water losses and the development of drought on all continents of the world [15, 48], thereby adversely affecting plant growth [18, 35, 50]. Some studies suggest that the positive influence of eCO_2 on vegetation growth can offset the negative impact of climatic drought, which can avoid further expansion of drylands [2, 48]. However, an increasing number of studies also show that the CO_2 fertilization effect is reduced by the limitation of water and nutrient conditions in the ecosystem [17, 34, 42, 44]. The observed data from meteorological stations show that since the

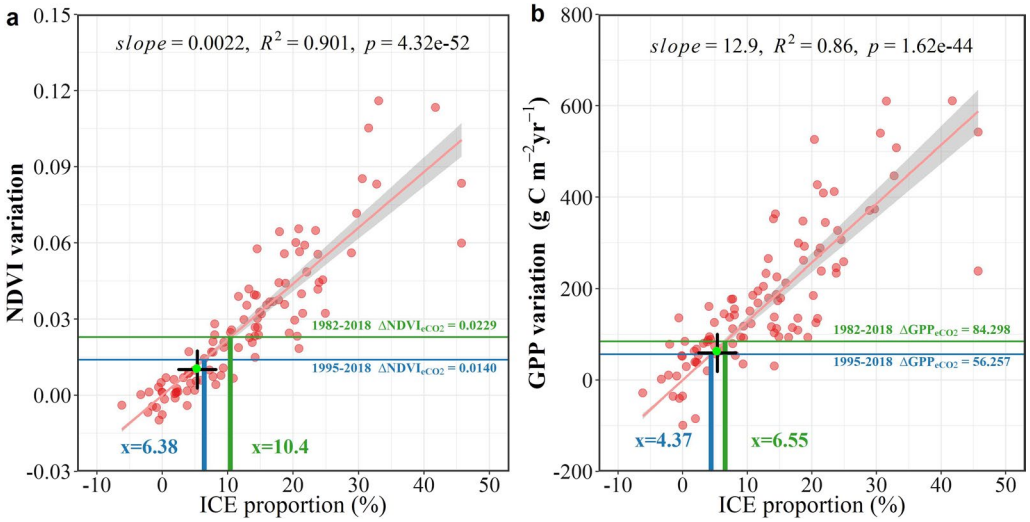

Fig. 5 Threshold of the ICE-driven NDVI and GPP variation ($\Delta NDVI_{ICE}$ and ΔGPP_{ICE}) outpace that of eCO_2. ICE proportion is the percentage of the change of irrigated cropland area to total vegetation area. **a** Relationship of the $\Delta NDVI_{ICE}$ and ICE proportion. **b** Relationship of the ΔGPP_{ICE} and ICE proportion. The shaded areas represent the 95% confidence intervals of the fitted curves. The red dots in the figure represent ICE proportion and $\Delta NDVI_{ICE}$ (ΔGPP_{ICE}) of different 0.75° grids in the region. The green dots represent ICE proportion and $\Delta NDVI_{ICE}$ (ΔGPP_{ICE}) between 1982 and 2018 in the whole region. The "+" represent ICE proportion and $\Delta NDVI_{ICE}$ (ΔGPP_{ICE}) between 1995 and 2018 in the whole region

1980s, the air temperature and precipitation in IANC have increased. The early precipitation trend is 2.00 mm/yr, and the later precipitation trend is 1.11 mm/yr, which decreased by 45% compared with the earlier period. However, the air temperature continued to rise, and the relative humidity increased significantly in the early period and decreased significantly in the later period. As a result, the regional climatic aridity intensified in more recent time (Additional file 1: Fig. S4). We found that as the relative humidity-driven NDVI and GPP trends changed from positive to negative, the fertilization effect of CO_2 on NDVI and GPP also decreased (Figs. 3d, e, f and 4d, e, f), although the atmospheric CO_2 concentration continued to increase (Fig. S6b). In the later period, the natural vegetation $\Delta NDVI_{eCO2}$ is 0.338 ± 0.094 (unit: 10^{-3} yr^{-1}) and the $\Delta NDVI_{RH}$ is − 0.15 ± 0.119 (ΔGPP_{eCO2} : 0.644 ± 0.550, ΔGPP_{RH}: -0.298 ± 0.568, unit: g C m^{-2} yr^{-1}, Figs. 3e and 4e). The fertilization effect of CO_2 alleviated the effect of drought, but its effect was not enough to alleviate the decline of NDVI and GPP trends. The trends of NDVI and GPP in cropland zone did not decrease as in natural vegetation zone, mainly due to the significant positive impact of ICE (Figs. 3d and 4d). The results of this paper show that in arid regions, it is ICE that mitigates the decline of vegetation growth trend, rather than the CO_2 fertilization effect, in the case of intensified climatic drought. In addition, over the entire region, the effect of ICE on the NDVI or GPP variation, was close to or even has outpaced that of eCO_2 at the late period (Figs. 3f and 4f). Our results indicate that the impact of ICE on vegetation growth has kept pace with the CO_2 fertilization effect in IANC, which is due to the significant increase in irrigated cropland area and the reduced effect of eCO_2 in the later years of the period under study.

In summary, ICE plays a significant role in the growth of vegetation in arid regions. We highlight the role of ICE, which on one hand confirms the importance of water availability in arid areas. Although the fertilization effect of CO_2 has a considerable impact on vegetation growth, the limitation of water conditions still predominates in arid regions [19, 32, 54]. On the other hand, we emphasize the impact of human activities on fragile ecosystems, which continuously challenge natural regulatory capacities. This finding is consistent with many other research results [4, 30].

ICE may exacerbate regional water conflicts in the future

The fertilization effect of CO_2 and human land use management promote regional vegetation growth, however, vegetation expansion, especially the increase of the afforestation and cropland, will exacerbate regional water conflicts in arid regions [8, 22]. In recent years, as the population grows rapidly and the demand for food increases, more and more land has been reclaimed. The data from the statistical yearbook show that the agricultural production in the northwest region has significantly increased, ensuring regional food security (Additional file 1: Fig. S14). More output means more water consumption, and agricultural water

consumption also significantly increases (Additional file 1: Fig. S14). For the total amount of water resources in the region remains stable, the increase of agricultural water use will inevitably crowd out ecological water use, which will lead to the cutoff of downstream inland rivers and the formation of more groundwater table drop funnels. Terrestrial water storage observations from NASA's Gravity Recovery and Climate Experiment (GRACE) satellite mission have revealed significant decline in regional water resources (Additional file 1: Fig. S14). The soil drought in some areas will intensify, and the natural vegetation will be affected and even face the threat of death, which will have an adverse impact on the regional ecology [14]. Facing the twofold pressure of water shortage and the adverse effects of climate change, maintaining an appropriate scale of irrigated cropland is critical for ensuring food security and ecological health in IANC in the future.

Assessment of data and methodological reliability

In this study, we employed multiple sources of data and a variety of methodologies to demonstrate the impact of natural factors and human activities on regional NDVI and GPP. To ensure the reliability and validity of our research findings, we conducted a comprehensive evaluation of the completeness and accuracy of the data, as well as the appropriateness of the methods. First, we utilized GIMMS3g NDVI and MOD13A3 NDVI data to study regional greenness variations and as input data for the LUE model. These data sets have been widely used and analyzed by many scholars and are broadly considered to have high reliability and representativeness [28, 41, 46, 50]. The driving data, such as climate data and atmospheric carbon dioxide concentration, are derived from authoritative observation organizations, ensuring high quality. Second, we integrated three machine learning algorithms to attribute NDVI, and subdivided larger grids into smaller ones to increase the data volume for training models, meeting the requirements of machine learning algorithms. The impacts of ICE on NDVI quantified by machine learning algorithms and trend decomposition methods are largely consistent, mutually validating each other. Finally, we used a revised LUE model to calculate GPP and attributed it. We collected real measurement data from four ground stations to validate the results of the improved LUE model, which showed that the LUE model performs well (Additional file 1: Fig. S10). Although there are certain limitations in the data and methods, we have taken measures to address them: (1) Some data have a short time range and can only be supplemented with other data to ensure the timeliness of the article. We have chosen data with consistent results for mutual verification and supplementation, and the supplementation period is short to ensure that it minimally impacts the main findings of our study. (2) The research objective of the text is to study the overall variation in regional vegetation growth indicators and their attribution. Using regional average values provides an overview of large-area trends, facilitating comparisons across the entire region, cropland zone, and natural vegetation zone. However, this approach lacks a more detailed and nuanced understanding of spatial variations, which should be addressed in future work through increased research on regional spatial changes.

Conclusions

Our results show that, from 1982 to 2018, vegetation growth was enhanced in IANC mainly under the influence of ICE and eCO_2, with ICE being the dominant factor in cropland zones. Since the mid-1990s, the significantly decreased regional relative humidity has negatively affected vegetation growth, and the CO_2 fertilization effects on NDVI and GPP also decreased. However, the irrigated cropland area has increased sharply, and its positive impact on vegetation growth approached or even exceeded that of eCO_2 in the later period, which has delayed the slowing down of the growth trend. In the whole region, the change of irrigated cropland area accounts for 5.25% of the total vegetation area, and the variation of GPP driven by ICE reached a level equivalent to that by eCO_2 at the late period when the ICE proportion reached 4.37%, while the ICE-driven NDVI variation will outpace the eCO_2 effect when the ICE proportion raises to above 6.38%. Although our study highlights the positive effect of irrigation cropland expansion on vegetation growth in arid areas, further expansion of irrigated cropland in the future will exacerbate regional conflict between water demand and supply, which may adversely affect the growth of natural vegetation. In the future, the ecological impact of ICE needs to be in-depth studied.

Supplementary Information

The online version contains supplementary material available at https://doi.org/10.1186/s12302-024-00852-6.

Additional file 1. Table S1. Dataset description. **Table S2**. Machine learning algorithms and their parameters. **Table S3**. Experiment station information for LUE model validation. **Figure S1**. Basic information of the IANC. **Figure S2**. Trend change point detection. **Figure S3**. Interannual variation of irrigated cropland area in IANC. **Figure S4**. Variations of air temperature, humidity climatic conditions in IANC. **Figure S5**. Comparison of MOD13A3 NDVI and GIMMS3g NDVI. **Figure S6**. Information of nitrogen application per unit area and atmospheric CO2 concentration. **Figure S7**. Calculate the effect of irrigated cropland expansion (ICE) on NDVI variation by trend decomposition method. **Figure S8**. Goodness of fit (R^2) of linear regression between simulated and measured values in the test set. **Figure S9**. Relationship between nitrogen fertilization and relative biomass. **Figure S10**. Revised LUE model validation. **Figure S11**. Comparison of

GPP estimate derived from revised LUE model and other GPP products in IANC. **Figure S12**. Attribution comparison of growing season NDVI trend by the different methods. **Figure S13**. GPP trend driven by various factors through the path of LUE item. **Figure S14**. Changes in total agricultural yield and regional total agricultural water consumption in the IANC.

Acknowledgements
Not applicable.

Author contributions
XL carried out the analysis and wrote the manuscript. SK contributed to the analysis and ideas and modified the paper. LZ, WD and MZ contributed ideas to the manuscript development and modified the paper. JN and JC contributed to the analysis. RD and SL provided the measured data of model validation.

Funding
We acknowledge financial supports by National Natural Science Foundation of China (51790534) and National Key R&D Program of China (2022YFD1900503).

Availability of data and materials
Data sources were provided with this paper in the Table S1 in the supplementary information.

Declarations

Ethics approval and consent to participate
Not applicable.

Consent for publication
Not applicable.

Competing interests
The authors declare no conflict of interests.

Author details
[1]State Key Laboratory of Efficient Utilization of Agricultural Water Resources, Beijing, China. [2]National Field Scientific Observation and Research Station On Efficient Water Use of Oasis Agriculture, Wuwei, China. [3]Center for Agricultural Water Research in China, China Agricultural University, Beijing, China. [4]State Key Laboratory of Water Resources Engineering and Management, Wuhan University, Wuhan, China. [5]CSIRO Environment, Canberra, Australia. [6]Lancaster Environment Centre, Lancaster University, Lancaster, UK.

Received: 12 September 2023 Accepted: 27 January 2024
Published online: 26 February 2024

References

1. Berdugo M et al (2020) Global ecosystem thresholds driven by aridity. Science 367(6479):787–790
2. Berg A, McColl KA (2021) No projected global drylands expansion under greenhouse warming. Nat Clim Chang 11(4):331-U71
3. Cai W et al (2014) large differences in terrestrial vegetation production derived from satellite-based light use efficiency models. Remote Sens 6:8945–8965
4. Chen C et al (2019) China and India lead in greening of the world through land-use management. Nat Sustain 2(2):122–129
5. de Jong R, Verbesselt J, Schaepman ME, de Bruin S (2012) Trend changes in global greening and browning: contribution of short-term trends to longer-term change. Glob Change Biol 18(2):642–655
6. Ding Z, Peng J, Qiu S, Zhao Y (2020) Nearly half of global vegetated area experienced Inconsistent vegetation growth in terms of greenness, cover, and productivity. Earths Future 8(10):e2020EF001618
7. Dusenge ME, Duarte AG, Way DA (2019) Plant carbon metabolism and climate change: elevated CO_2 and temperature impacts on photosynthesis, photorespiration and respiration. New Phytol 221(1):32–49
8. Feng X et al (2016) Revegetation in China's loess plateau is approaching sustainable water resource limits. Nat Clim Chang 6(11):1019–1022
9. Fensholt R et al (2012) Greenness in semi-arid areas across the globe 1981–2007 — an earth observing satellite based analysis of trends and drivers. Remote Sens Environ 121:144–158
10. Field CB, Randerson JT, Malmström CM (1995) Global net primary production: combining ecology and remote sensing. Remote Sens Environ 51(1):74–88
11. Forzieri G, Alkama R, Miralles Diego G, Cescatti A (2017) Satellites reveal contrasting responses of regional climate to the widespread greening of Earth. Science 356(6343):1180–1184
12. Gan R et al (2021) Estimating ecosystem maximum light use efficiency based on the water use efficiency principle. Environ Res Lett 16(10):104032
13. Gonsamo A et al (2021) Greening drylands despite warming consistent with carbon dioxide fertilization effect. Glob Change Biol 27(14):3336–3349
14. Green JK et al (2019) Large influence of soil moisture on long-term terrestrial carbon uptake. Nature 565(7740):476–479
15. Huang J, Yu H, Guan X, Wang G, Guo R (2016) Accelerated dryland expansion under climate change. Nat Clim Chang 6(2):166–171
16. Ise T, Litton CM, Giardina CP, Ito A (2010) Comparison of modeling approaches for carbon partitioning: Impact on estimates of global net primary production and equilibrium biomass of woody vegetation from MODIS GPP. J Geophys Res-Biogeosci. https://doi.org/10.1029/2010JG001326
17. Jin Z, Ainsworth EA, Leakey ADB, Lobell DB (2018) Increasing drought and diminishing benefits of elevated carbon dioxide for soybean yields across the US Midwest. Glob Change Biol 24(2):e522–e533
18. Konings AG, Williams AP, Gentine P (2017) Sensitivity of grassland productivity to aridity controlled by stomatal and xylem regulation. Nat Geosci 10(4):284–288
19. Lemordant L, Gentine P, Swann AS, Cook BI, Scheff J (2018) Critical impact of vegetation physiology on the continental hydrologic cycle in response to increasing CO2. Proc Natl Acad Sci USA 115(16):4093–4098
20. Lewis SL, Wheeler CE, Mitchard ETA, Koch A (2019) Regenerate natural forests to store carbon. Nature 568(7750):25–28
21. Li J, Peng S, Li Z (2017) Detecting and attributing vegetation changes on China's Loess Plateau. Agric For Meteorol 247:260–270
22. Liu Y et al (2022) Effects of global greening phenomenon on water sustainability. CATENA 208:105732
23. Lu C, Tian H (2016) Half-degree gridded nitrogen and phosphorus fertilizer use for global agriculture production during 1900–2013, Supplement to: Lu, C; Tian, H (2017): Global nitrogen and phosphorus fertilizer use for agriculture production in the past half century: shifted hot spots and nutrient imbalance. Earth Syst Sci Data 9(1):181–192. https://doi.org/10.5194/essd-9-181-2017.PANGAEA
24. Malhi Y et al (2015) The linkages between photosynthesis, productivity, growth and biomass in lowland Amazonian forests. Glob Change Biol 21(6):2283–2295
25. Mueller ND et al (2012) Closing yield gaps through nutrient and water management. Nature 490(7419):254–257
26. Nemani Ramakrishna R et al (2003) Climate-driven increases in global terrestrial net primary production from 1982 to 1999. Science 300(5625):1560–1563
27. Novick KA et al (2016) The increasing importance of atmospheric demand for ecosystem water and carbon fluxes. Nat Clim Chang 6(11):1023–1027
28. Pan N et al (2018) Increasing global vegetation browning hidden in overall vegetation greening: insights from time-varying trends. Remote Sens Environ 214:59–72
29. Pei Y et al (2022) Evolution of light use efficiency models: improvement, uncertainties, and implications. Agric For Meteorol 317:108905
30. Peng Q, Wang RH, Jiang YL, Li C (2021) Contributions of climate change and human activities to vegetation dynamics in Qilian Mountain National Park, northwest China. Glob Ecol Conserv 32:e01947

31. Piao S et al (2011) Changes in satellite-derived vegetation growth trend in temperate and boreal Eurasia from 1982 to 2006. Glob Change Biol 17(10):3228–3239
32. Piao S et al (2020) Characteristics, drivers and feedbacks of global greening. Nat Rev Earth Environ 1(1):14–27
33. Piao S et al (2015) Detection and attribution of vegetation greening trend in China over the last 30 years. Glob Change Biol 21(4):1601–1609
34. Reich PB, Hobbie SE, Lee TD (2014) Plant growth enhancement by elevated CO_2 eliminated by joint water and nitrogen limitation. Nat Geosci 7(12):920–924
35. Restaino Christina M, Peterson David L, Littell J (2016) Increased water deficit decreases Douglas fir growth throughout western US forests. Proc Natl Acad Sci 113(34):9557–9562
36. Ryu Y, Berry JA, Baldocchi DD (2019) What is global photosynthesis? History, uncertainties and opportunities. Remote Sens Environ 223:95–114
37. Sánchez ML, Pardo N, Pérez IA, García MA (2015) GPP and maximum light use efficiency estimates using different approaches over a rotating biodiesel crop. Agric For Meteorol 214–215:444–455
38. Smith WK et al (2016) Large divergence of satellite and earth system model estimates of global terrestrial CO2 fertilization. Nat Clim Chang 6(3):306–310
39. Suding K et al (2015) Committing to ecological restoration. Science 348(6235):638–640
40. Tong X et al (2018) Increased vegetation growth and carbon stock in China karst via ecological engineering. Nat sustain 1(1):44–50
41. Wan W et al (2022) Spatiotemporal patterns of maize drought stress and their effects on biomass in the Northeast and North China Plain from 2000 to 2019. Agric For Meteorol 315:108821
42. Wang S et al (2020) Recent global decline of CO_2 fertilization effects on vegetation photosynthesis. Science 370(6522):1295–1300
43. Wang XH et al (2021) Global irrigation contribution to wheat and maize yield. Nat Commun 12(1):1235
44. Winkler AJ et al (2021) Slowdown of the greening trend in natural vegetation with further rise in atmospheric CO_2. Biogeosciences 18(17):4985–5010
45. Wu D et al (2020) Accelerated terrestrial ecosystem carbon turnover and its drivers. Glob Change Biol 26(9):5052–5062
46. Wu DH et al (2015) Time-lag effects of global vegetation responses to climate change. Glob Change Biol 21(9):3520–3531
47. Xu HJ, Wang XP, Zhao CY, Zhang XX (2019) Responses of ecosystem water use efficiency to meteorological drought under different biomes and drought magnitudes in northern China. Agric For Meteorol 278:107660
48. Xu L et al (2021) Multifaceted characteristics of dryland aridity changes in a warming world. Nat Rev Earth Environ 2(4):232–250
49. Yao Y et al (2014) Bayesian multimodel estimation of global terrestrial latent heat flux from eddy covariance, meteorological, and satellite observations. J Geophys Res Atmos 119(8):4521–4545
50. Yuan W et al (2019) Increased atmospheric vapor pressure deficit reduces global vegetation growth. Sci Adv 5(8):eaax1396
51. Zeng N et al (2014) Agricultural green revolution as a driver of increasing atmospheric CO_2 seasonal amplitude. Nature 515(7527):394–397
52. Zhang J, Fu B, Stafford-Smith M, Wang S, Zhao W (2021) Improve forest restoration initiatives to meet sustainable development goal 15. Nat Ecol Evolut 5(1):10–13
53. Zhang L-X, Zhou D-C, Fan J-W, Hu Z-M (2015) Comparison of four light use efficiency models for estimating terrestrial gross primary production. Ecol Model 300:30–39
54. Zhang Y et al (2022) Increasing sensitivity of dryland vegetation greenness to precipitation due to rising atmospheric CO_2. Nat Commun 13(1):4875
55. Zhang YL, Song CH, Band LE, Sun G (2019) No proportional increase of terrestrial gross carbon sequestration from the greening earth. J Geophys Res Biogeosci 124(8):2540–2553
56. Zhu Z et al (2016) Greening of the earth and its drivers. Nat Clim Chang 6(8):791–795

Publisher's Note

Springer Nature remains neutral with regard to jurisdictional claims in published maps and institutional affiliations.